
Optimal precision for GANs

Thibaut Issenhuth

Criteo AI Labs, Ecole des Ponts, CNRS
t.issenhuth@criteo.com

Ugo Tanielian

Criteo AI Labs
u.tanielian@criteo.com

Jérémie Mary

Criteo AI Labs
j.mary@criteo.com

David Picard

Ecole des Ponts, UGE, CNRS
david.picard@enpc.fr

Abstract

When learning disconnected distributions, Generative adversarial networks (GANs) are known to face model misspecification. Indeed, a continuous mapping from a unimodal latent distribution to a disconnected one is impossible, so GANs necessarily generate samples outside of the support of the target distribution. This raises a fundamental question: what is the latent space partition that minimizes the measure of these areas? Building on a recent result of geometric measure theory, we prove that an optimal GANs must structure its latent space as a 'simplicial cluster' - a Voronoi partition where cells are convex cones - when the dimension of the latent space is larger than the number of modes. In this configuration, each Voronoi cell maps to a distinct mode of the data. We derive both an upper and a lower bound on the optimal precision of GANs learning disconnected manifolds. Interestingly, these two bounds have the same order of decrease: $\sqrt{\log m}$, m being the number of modes. Finally, we perform several experiments to exhibit the geometry of the latent space and experimentally show that GANs have a geometry with similar properties to the theoretical one.

1 Introduction

GANs (Goodfellow et al., 2014), a family of deep generative models, have shown great capacities to generate photorealistic images (Karras et al., 2019). State-of-the-art models, like StyleGAN (Karras et al., 2019) or TransformerGAN (Jiang et al., 2021), show empirical benefits from relying on overparametrized networks with high-dimensional latent spaces. Besides, manipulating the latent representation of a GAN is also helpful for diverse tasks such as image editing (Shen et al., 2020; Wu et al., 2021) or unsupervised learning of image segmentation (Abdal et al., 2021). However, there is still a poor theoretical understanding of how GANs organize the latent space. We argue that this is a crucial step in apprehending the behavior of GANs better.

To better understand GANs, the setting of disconnected distributions learning is enlightening. Experimental and theoretical works (Khayatkhoei et al., 2018; Tanielian et al., 2020) have shown a fundamental limitation of GANs when dealing with such distributions. Since the distribution modeled by any GANs is connected, some areas of GANs' support are mapped outside the true data distribution. To measure the ability of GANs to generate high-quality samples, practitioners have developed the *precision* (Sajjadi et al., 2018; Kynkäänniemi et al., 2019) and the *density* (Naeem et al., 2020) metric quantifying the portion of generated points belonging to the support of the target distribution. When covering many modes of the target distribution, GANs necessarily have limited precision and/or density: this is due to the portion of generated points that do not belong to the support of the target distribution.

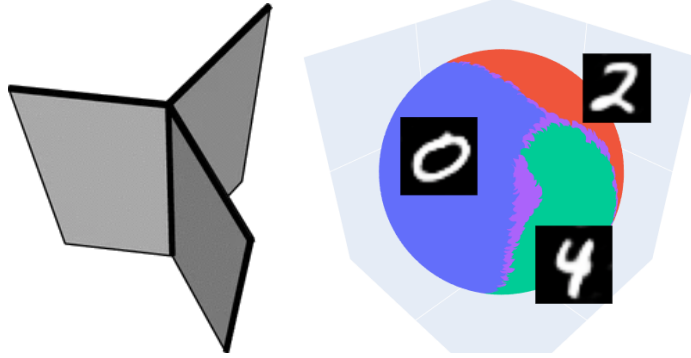


Figure 1: Illustration of the ability of GANs to find an optimal configuration in the latent space. On the left, the propeller shape is a partition of 3D Gaussian space with the smallest gaussian-weighted perimeter (figure from Heilman et al. (2013)). On the right, we show the 3D Gaussian latent space of a GAN trained on three classes of MNIST. Each area colored in blue, green, or red maps samples in one of the three classes. In purple, we observe the samples that are classified with low confidence. We see that the partition reached by the GAN (right) is close to optimality (left).

We argue that optimality in GANs is closely linked to their latent space geometry. In particular, we make the connection between optimality in GANs and Gaussian isoperimetric (Ledoux, 1996) theory aiming at splitting the Gaussian space with the minimal perimeter. As long as the dimension is greater than the number of modes, we identify a specific latent space configuration where the generator maximizes its precision: a 'simplicial cluster' obtained as the Voronoi cells of equidistant points (see left of Figure 1). This enables us to derive both an upper and a lower bound on the precision of GANs. To summarize, our contributions are the following:

- Many evaluation metrics have been proposed to evaluate GANs. We first prove an asymptotic connection between the improved precision/recall (Kynkäänniemi et al., 2019) and density/coverage (Naeem et al., 2020) metrics, thus motivating the use of a unified metric.
- We derive a new theoretical analysis, stating both an upper-bound and a lower-bound on the precision of GANs. We stress that specific latent configurations allow the generator to maximize its precision. When the number of modes is inferior to the latent dimension, the upper and lower-bounds decrease in $\sqrt{\log m}$, where m is the number of modes, showing that GANs can approach the optimal precision. However, when the latent dimension d is lower than the number of modes m , the lower-bound is of order $\log(d) + O\left(\frac{m}{d \log(d)}\right)$.
- Experimentally, we show that GANs tend to structure their latent space as 'simplicial clusters' on image datasets. We explore two properties of the latent space: linear separability and convexity of classes. Playing with the latent space dimension of GANs, we also highlight the two regimes derived from the theoretical analysis.

2 Related Work

2.1 Notation

Data. We assume that the target distribution μ_* is defined on Euclidean space \mathbb{R}^D (potentially a high-dimensional space), equipped with the norm $\|\cdot\|$. We denote S_{μ_*} the support of this unknown distribution μ_* . In practice, however, we only have access to a finite collection of i.i.d. observations X_1, \dots, X_n distributed according to μ_* . Thus, for the remainder of the article, we let μ_n be the empirical measure based on X_1, \dots, X_n .

Generative model. We consider \mathcal{G}_L the set of L -Lipschitz continuous functions from the latent space \mathbb{R}^d to the high-dimensional space \mathbb{R}^D . Each generator aims at producing realistic samples. The latent space distribution defined on \mathbb{R}^d , is supposed to be Gaussian and is noted γ . Thus, each candidate distribution is the pushforward between γ and a generator G and is noted as $G\#\gamma$.

This Lipschitzness assumption on \mathcal{G}_L is reasonable since [Virmaux and Scaman \(2018\)](#) has shown and presented an algorithm that upper-bounds the Lipschitz constant of any deep neural network. In practice, one can enforce the Lipschitzness of generator functions by clipping the neural networks’ parameters ([Arjovsky et al., 2017](#)), penalizing the discriminative functions’ gradient ([Gulrajani et al., 2017](#); [Kodali et al., 2017](#); [Wei et al., 2018](#); [Zhou et al., 2019](#)), or penalizing the spectral norms ([Miyato et al., 2018](#)). Note that some large-scale generators such as SAGAN ([Zhang et al., 2019](#)) and BigGAN ([Brock et al., 2019](#)) also make use of spectral normalization for the generator.

2.2 GANs and disconnected distributions

A significant flaw of GANs ([Goodfellow et al., 2014](#)) is their difficulty in learning multi-modal distributions. This phenomenon has been deeply analyzed by [Khayatkhoei et al. \(2018\)](#); [Tanielian et al. \(2020\)](#). The problem comes from this fundamental trade-off: GANs can either cover all modes and generate out-of-manifold samples, generate only good quality samples, or neglect some modes. Some methods proposed ways to train disconnected generators ([Khayatkhoei et al., 2018](#); [Gurumurthy et al., 2017](#)), but with little benefits compared to single overparametrized generators with rejection mechanisms ([Tanielian et al., 2020](#); [Azadi et al., 2018](#)).

Empirically, different works give intuition on the latent space structure of GANs. [Karras et al. \(2019\)](#) showed that binary attributes are linearly separable in the gaussian latent space and are better separated in an intermediate latent space. [Shen et al. \(2020\)](#) stress that face attributes are separated by hyperplanes and edit images by moving in the latent space orthogonally to these hyperplanes. Finally, [Härkönen et al. \(2020\)](#) shows that keeping principal components from a PCA in the intermediate latent space of StyleGAN captures most variance of the model, which implies that GANs compress the high-dimensional latent space. Another line of research consists of regarding the latent space of generative models with a Riemannian perspective and defining a metric tensor using the generator’s Jacobian. [Arvanitidis et al. \(2018\)](#) and [Chen et al. \(2018a\)](#) use this metric to find the shortest paths on the data manifold.

However, these findings might not be sufficient for a clear understanding of the required geometry of the latent space. For instance, [Karras et al. \(2019\)](#) use a huge latent space dimension (\mathbb{R}^{512}), while [Sauer et al. \(2022\)](#) arguing that the optimal latent space dimension is close to the intrinsic dimension of images (\mathbb{R}^{64} for ImageNet). [Tanielian et al. \(2020\)](#) stress the relevance of this problem by showing that the precision of GANs can converge to 0 when the number of modes or the distance between them increases. In this paper, we make a step towards a better understanding of the behavior of GANs and explicit an optimal latent space configuration when the number of modes m is smaller than the dimension of the latent space d .

2.3 Evaluation of GANs

When learning disconnected manifolds, [Sajjadi et al. \(2018\)](#) illustrated the need to measure simultaneously the quality and the diversity of the samples generated to identify the mode collapse. To do so, they propose using the Precision/Recall metric.

Precision/Recall: The key intuition is that precision should quantify how much of the fake distribution can be generated by the true distribution, while recall measures how much of the true distribution can be reconstructed by the model distribution. [Kynkäänniemi et al. \(2019\)](#) highlighted an important drawback of this PR metric: it cannot correctly interpret situations when large numbers of samples are packed together. For the need of this paper, we only consider $\bar{\alpha}$ (respectively $\bar{\beta}$) the maximum attainable precision (respectively recall). [Sajjadi et al. \(2018, Theorem 1\)](#) proves that:

$$\bar{\alpha} = G_{\#}^{\dagger}\gamma(S_{\mu^*}) \quad \text{and} \quad \bar{\beta} = \mu^*(S_{G_{\#}^{\dagger}\gamma}) \tag{1}$$

More recently, [Naeem et al. \(2020\)](#) have shown that the Precision/Recall metric ([Sajjadi et al., 2018](#)) and its improved version ([Kynkäänniemi et al., 2019](#)) are not robust to outlier samples of both the target and the generated distribution. To correct this and fix the overestimation of the manifold around real outliers, [Naeem et al. \(2020\)](#) propose the Density/Coverage metric.

Density/Coverage: Instead of counting how many fake samples belong to a real sample neighbourhood, density counts how many real sample neighbourhoods contain a generated sample. In particular,

for two finite sample datasets $D_X = (X_1, \dots, X_n)$ (real data), $D_G = (G(z_1), \dots, G(z_m))$ (fake data) and any $k \in \mathbb{N}$, the density is defined as:

$$\delta_k := \frac{1}{km} \sum_{j=1}^m \sum_{i=1}^n \mathbb{1}_{\{G(z_j) \in B_k(X_i)\}}$$

where $B_k(X)$ refers to the set of k nearest neighbors of X w.r.t. the Euclidean distance. Coverage counts the number of real sample neighbourhoods that contain at least one fake sample:

$$\lambda_k := \frac{1}{N} \sum_{i=1}^N \mathbb{1}_{\{\exists j \in [1, M], G(z_j) \in B_k(X_i)\}}$$

A first contribution is to formalize both the density and the coverage and make the link with the Precision/Recall metric (Sajjadi et al., 2018). Interestingly, we can show the following result:

Theorem 1. *Let μ^* be the target distribution and $D_X = (X_1, \dots, X_n)$ (real data) be sampled from μ^* . Let $D_G = (G(z_1), \dots, G(z_m))$ (fake data). Let (k, n) be such that $\frac{k}{\log(n)} \rightarrow 0$ and $\frac{k}{n} \rightarrow 0$. Then*

$$i) \quad \delta_k \leq \bar{\alpha} c_D \text{ a.s. where } c_D \text{ is a constant function of the dimension } D \quad (2)$$

$$ii) \quad \lambda_k \xrightarrow{k \rightarrow \infty} \bar{\beta} \text{ a.s.,} \quad (3)$$

where S_{μ^*} refers to the support of the random variable μ^* .

Contrary to the Improved PR metric (Kynkäänniemi et al., 2019) that has been shown (Tanielian et al., 2020, Theorem 1) to be asymptotically equivalent to PR metric (Sajjadi et al., 2018), it is not clear here whether the density is asymptotically equivalent to precision. In particular, it is not known whether the bound (2) is tight or whether the density could be greater than 1. If the density was changed to a formulation closer to the coverage, i.e. $\frac{1}{m} \sum_{j=1}^m \mathbb{1}_{\{\exists i \in [1, n], \{G(z_j) \in B_k(X_i)\}\}}$, then we could show that it is smaller than 1 and it converges towards $\bar{\alpha}$.

3 Optimal precision in GANs

In this section, we want to better understand the latent space of GANs by explicating which are the GANs with the highest precision under constraints of recall. For the present section, we will use the notion of precision and recall defined in (1). Using this definition allows us to circumvent the non-parametric estimators involved in the existing metrics (Kynkäänniemi et al., 2019; Naeem et al., 2020). Thus, for a given generator G , the precision α_G and the recall β_G are obtained as follows:

$$\alpha_G = \bar{\alpha} = G_{\#} \gamma(S_{\mu_n}) \quad \text{and} \quad \beta_G = \bar{\beta} = \mu_n(S_{G_{\#} \gamma}).$$

Note that each GAN is the pushforward distribution of a unimodal (connected) Gaussian distribution γ and a continuous function G . Consequently, the modeled generative distribution $G_{\#} \gamma$ will have connected support. When learning disconnected manifolds or when training a GAN in a few-shot learning setting, this necessarily maps fake data points out of the true manifold. This leads us to the following question, given that a generator has its recall equal to 1, what is its maximum precision?

3.1 Definition of the problem

First, let us assume that the target distribution is composed of disconnected manifolds, which is a reasonable assumption for real-word distributions.

Assumption 1. *The target distribution μ_* is disconnected and composed of m distinct manifolds M_i .*

Now, to set the problem better, we create the connection between any generator $G \in \mathcal{G}_L$ and a given partition \mathcal{A} of the Gaussian space \mathbb{R}^d .

Definition 1. *For a given partition $\mathcal{A} = \{A_1, \dots, A_m\}$ on \mathbb{R}^d , we note $\mathcal{G}_L^{\mathcal{A}} \subset \mathcal{G}_L$ the set of L -Lipschitz generators associated with \mathcal{A} verifying, for all $G \in \mathcal{G}_L^{\mathcal{A}}$:*

$$\forall i \in [1, m], \forall z \in A_i, i = \arg \min_{i \in [1, m]} \|G(z) - M_i\|.$$

Consequently, each given generator is associated to a unique partition in the latent space that partly explains its behavior. We say that the generator is *well-balanced* if it is associated with a partition $\mathcal{A} = \{A_1, \dots, A_m\}$ on \mathbb{R}^d verifying $\gamma(A_1) = \dots = \gamma(A_m) = 1/m$.

We are currently interested in maximizing the precision of generative models. Any points in the intersection of two cells $A_i \cap A_j$, $(i, j) \in [1, m]^2$ do not belong to any existing modes. Besides, due to the generator's Lipschitzness, there is a small neighborhood of the boundary such that any points will be mapped out of the target manifold. This region in the latent space thus reduces the precision. For a given $\varepsilon > 0$, we now define the epsilon-boundary of the partition \mathcal{A} as follows:

Definition 2. For a given partition $\mathcal{A} = \{A_1, \dots, A_m\}$ of \mathbb{R}^d and a given $\varepsilon \in \mathbb{R}_+^*$, we denote $\partial^\varepsilon \mathcal{A}$ the epsilon-boundary of \mathcal{A} . It is defined as follows:

$$\partial^\varepsilon \mathcal{A} = \bigcup_{i=1}^m (\cup_{j \neq i} A_j)^\varepsilon \setminus (\cup_{j \neq i} A_j),$$

where A^ε corresponds to the ε -extension of set A . To better understand the link between this epsilon-boundary of \mathcal{A} and the precision of any generator in $\mathcal{G}_{\mathcal{A}}$, one can show the following lemma:

Lemma 1. Assume that Assumption 1 is satisfied and $\mathcal{A} = \{A_1, \dots, A_m\}$ is a partition with $\gamma(A_1) = \dots = \gamma(A_m) = 1/m$. Then, for any well-balanced generator $G \in \mathcal{G}_L^{\mathcal{A}}$ verifying $\beta_G = 1$, we have:

$$\alpha_G \leq 1 - \partial^{\varepsilon_{\min}} \mathcal{A}, \quad \text{where } \varepsilon_{\min} = \min_{i \in [1, m], j \neq i} \frac{\|M_i - M_j\|}{L}. \quad (4)$$

Consequently, to better determine the precision of generative models, one might be interested in determining the measure of this epsilon-boundary $\partial^\varepsilon \mathcal{A}$. In particular, we argue that finding the generative models with the highest precision levels is closely linked to finding the partition of the Gaussian space with the smallest epsilon-boundary measures $\gamma(\partial^\varepsilon \mathcal{A})$. This is tightly connected to the theoretical field of Gaussian isoperimetric inequalities.

3.2 Optimality in GANs.

Isoperimetric inequalities link the measure of sets with their perimeters. More specifically, isoperimetric inequalities highlight minimizers of the perimeter for a fixed measure, *e.g.* the sphere in an euclidean space with Lebesgue measure. Gaussian isoperimetric inequalities study this problem in Gaussian space. Ledoux (1996, Theorem 1.3) shows that in a finite-dimensional Gaussian space, among all sets of a given measure, half-spaces have a minimal weighted perimeter. More formally, for any Borel set A in \mathbb{R}^d and a half-space H , if we have $\gamma(A) \geq \gamma(H)$, then $\gamma(A^\varepsilon) \geq \gamma(H^\varepsilon)$ for any $\varepsilon > 0$, where A^ε denotes the ε -extension of the set A .

The Gaussian multi-bubble conjecture was formulated when looking for a way to partition the Gaussian space with the least-weighted perimeter. It was recently proved by Milman and Neeman (2022) who showed that the best way to split a Gaussian space \mathbb{R}^d in m clusters of equal measure, with $2 \leq m \leq d + 1$, is by using "simplicial clusters" obtained as the Voronoi cells of m equidistant points in \mathbb{R}^d . Convex geometry theory tells us that the boundary is the union of m convex cones, each of them contained in a distinct hyperplane that goes through the origin of \mathbb{R}^d . We note \mathcal{A}^* any partition corresponding to this optimal configuration, see Figure 1. In the present paper, we mainly propose to adapt this result to the community of GANs via the following theorems.

Maximal precision of GANs. Using results from Gaussian isoperimetric inequalities (Schechtman, 2012), we derive an upper bound on the maximal precision of generative models:

Corollary 1. Assume that Assumption 1 is satisfied. Let L, d be such that $L \geq d \sqrt{\log(m)}$. Then, for any well-balanced generator $G \in \mathcal{G}_L$ verifying $\beta_G = 1$, we have:

$$\alpha_G \leq 1 - \varepsilon_{\min} (1 - \varepsilon_{\min} \sqrt{2 \log(m)}) / (\sqrt{2\pi}) \quad (5)$$

This result has to be put into perspective with the result obtained by Tanielian et al. (2020, Theorem 3), which showed a similar result when the number of modes increases:

$$\alpha_G \stackrel{m \rightarrow \infty}{\leq} e^{-\frac{1}{8} \varepsilon_{\min}^2} e^{-\varepsilon_{\min} \sqrt{\log(m)/2}} \quad (6)$$

Interestingly, the bound in (5) gives an interesting insight when the number of modes increases in a finite-sample setting. Also, we observe that when $m \rightarrow \infty$, both (5) and 6 give similar results.

Optimal precision of GANs. We are now trying to understand whether the bound in the Corollary 1 is tight. To do so, we are looking for generative models with optimal levels of precision. We argue that, in the case where $m \leq d + 1$, such models are closely linked to the optimal partitions \mathcal{A}^* derived in the Gaussian Multi-Bubble conjecture and proven to be optimal by [Milman and Neeman \(2022\)](#). In the following, with a slight abuse of notation, we note M_i the center of each mode. We define $G_\varepsilon^* \in \mathcal{G}_L$ ($\varepsilon > 0$) be a generative model associated with $\mathcal{A}^* = (A_1, \dots, A_m)$ such that:

$$G_\varepsilon^*(z) = \sum_{i \in S_z} w_i(z) M_i, \quad \text{with } w_i(z) = \frac{d(z, (A_i^\varepsilon)^c)}{\sum_{j \in S_z} d(z, (A_j^\varepsilon)^c)} \quad (7)$$

where $d(z, A) = \min_{x \in A} \|z - x\|$, and $S_z = \{j \in [1, m] \text{ such that } z \in A_j^\varepsilon\}$ denotes the set of cell-extensions the point z belongs to.

We can see that $G_\varepsilon^* \# \gamma$ memorizes the dataset since every z close to the center of the cell A_i such that $|S_z| = 1$ verifies $G_\varepsilon^*(z) = M_i$. To be more precise, all samples are mapped to one of the centers $M_i, i \in [1, m]$, except for those in ε -boundaries. When z belongs to the intersection of two ε -boundaries, $G_\varepsilon^*(z)$ is a simple linear combination of 2 points. It is only when $|S_z| \geq 3$ that more complex samples are generated. A simple illustration of G_ε^* for $d = 2$ and $m = 3$ is given in Appendix.

The definition of G_ε^* is motivated by the following theorem, where we note

$$D = \max_{(i,j)} \|M_i - M_j\| \quad \text{and} \quad \varepsilon_{\max} = \max_{i \in [1,m], j \neq i} \frac{\|M_i - M_j\| \sqrt{m}}{L}.$$

Theorem 2 (Optimality of G_ε^*). *Assume that Assumption 1 is satisfied. Then, for any $L > D$, $G_{\varepsilon_{\max}}^*$ is a well-balanced generator in \mathcal{G}_L verifying $\beta_{G_{\varepsilon_{\max}}^*} = 1$ and such that*

$$1 - \partial^{\varepsilon_{\min}} \mathcal{A}^* \geq \alpha_{G_{\varepsilon_{\max}}^*} \geq 1 - \partial^{\varepsilon_{\max}} \mathcal{A}^*.$$

Now, let $m \leq d + 1$. For any $\delta > 0$, if L is large enough, then, for any well-balanced $G \in \mathcal{G}_L$ verifying $\beta_G = 1$ we have:

$$\alpha_G \leq \alpha_{G_{\varepsilon_{\max}}^*} + \delta$$

This theorem, which proof is delayed to Appendix, shows that G_ε^* is optimal w.r.t. the precision metric. Interestingly, one can also show that the image of G_ε^* is equal to the convex hull of the centers $M_i, i \in [1, m]$ (proof in Appendix too). In particular, there exists a particularly interesting neighborhood v of 0 where $G_\varepsilon^*(v)$ is equal to the whole convex hull of the centers $M_i, i \in [1, m]$. We are now ready to state the lower-bound equivalent of Corollary 1:

Corollary 2. $\forall L \geq D\sqrt{m}$, there exists a well-balanced generator $G \in \mathcal{G}_L$ verifying $\beta_G = 1$ with

$$\alpha_G \geq 1 - \frac{\varepsilon_{\max} \sqrt{\pi \log(m)}}{\sqrt{2}} + O\left(\frac{\varepsilon_{\max} \log(m)}{m}\right), \quad \text{when } m \leq d$$

$$\alpha_G \geq 1 - \frac{\varepsilon_{\max} \log(d)}{\sqrt{2\pi}} + O\left(\frac{m}{d \log(d)}\right), \quad \text{when } m > d.$$

For the sake of clarity, the proof is delayed to appendix. The bound in Corollary 2 has been extended to the case $d < m + 1$ where the optimal partition is unknown using results from ([Boland and Urrutia, 1995](#)). We see that when the number of modes is less than the number of dimensions in the latent space, the only factor that impacts the precision is the number of modes. Note that for $m > d$ but $m/d \ll d$, the bound changes from $\sqrt{\log(d)}$ to $\log(d)$.

4 Experiments: understanding the latent space

In the following experiments, we validate our theoretical analysis and derive insights for GANs trained on image datasets. First, we verify if the latent space geometry of GANs has properties similar to the ones of the least Gaussian-weighted perimeter obtained by [Milman and Neeman \(2022\)](#). Second, we vary the number of latent dimensions of GANs to observe the phase transition of our Corollary 2. To disentangle the number of modes from the intrinsic dimension of the data manifold, we construct low-dimensional disconnected datasets with conditional GANs.

Dataset	Precision	LogReg Accuracy	Convex Accuracy
MNIST	93.2	90.4	98.7
CIFAR-3	80.9	78.7	95.6
CIFAR-10	74.0	64.0	74.4
CIFAR-100	66.5	25.1	42.0

Table 1: In this experiment, we verify 1) if the latent spaces of GANs are linearly separable (LogReg Accuracy); 2) if each cell of the latent space is convex. (Convex Accuracy). In par with Theorem 2, the higher the precision is, the more each cell in the latent space is linearly separable and convex.

We train GANs with a Wasserstein loss and gradient penalty in all our experiments (Arjovsky et al., 2017; Gulrajani et al., 2017). On the MNIST dataset (LeCun et al., 1998), both generator and discriminator are based on standard convolutional architectures. On CIFAR-3, CIFAR-10 and CIFAR-100 datasets (Krizhevsky et al., 2009), we use a Resnet-based (He et al., 2016) convolutional architecture with self-modulation in the generator (Chen et al., 2018b), *i.e.* batch normalization conditioned to a learned transformation of the latent vector. CIFAR-3 is composed of *horse*, *car* and *boat* classes from CIFAR-10. Implementation details and code are given in Appendix.

4.1 Expliciting the latent space geometry of GANs

Milman and Neeman (2022) show that the optimal configuration in the latent space is obtained as the Voronoi cells of m equidistant points in \mathbb{R}^d . This means that if GANs reach this optimal configuration, each of the cells (mapping to different modes) must be *convex polytopes* and thus verify the following properties: 1) each cell has 'flat' sides, and are bounded exclusively by faces; 2) each cell is convex. In the following experiments, we study whether GANs' latent spaces feature these two properties.

Are classes linearly separable in the latent space of GANs? To begin with, we leverage a labeled dataset and investigate if a simple linear model (*e.g.*, multinomial logistic regression) can map latent space to label space. If each cell in the latent space is bounded by faces (and is thus linearly separable), the linear model is expected to be a good predictor of a generated sample's label.

Let us consider a labeled dataset of samples with a fixed number of classes. Let G_θ be a pre-trained generator, and C_ϕ a pre-trained classifier considered as an oracle. Using G_θ and C_ϕ , we construct a dataset of latent vectors $z \in \mathbb{R}^d$ and their associated labels $y = C_\phi(G_\theta(z))$. This dataset is later split into 100k training points and 10k test points. On CIFAR-10 and CIFAR-100 datasets, low-quality samples with the lowest confidence scores have also been removed from the dataset.

The mapping from latent vectors z to their labels y is learned by a multinomial logistic regression. We report the test-set results in Table 1 under the column *LogReg Accuracy*. This accuracy reaches 90% on MNIST and 64% on CIFAR-10. Interestingly, there is also a correlation between the linear separability of the latent space and the precision metric, which validates the optimality of the simplicial cluster partition. The higher the precision, the more the latent space seems to be linearly separable.

Are classes convex in the latent space of GANs? In this experiment, we draw two random latent vectors z_0 and z_1 that belong to the same class. Then, we generate linear interpolations $z_\varepsilon = \varepsilon z_0 + (1 - \varepsilon)z_1$ and verify if these new samples belong to the same class as z_0 and z_1 , *i.e.* whether $C_\phi(G_\theta(z_\varepsilon))$ equals to $C_\phi(G_\theta(z_0))$. We report the mean accuracy of this experiment in Table 1 under the column *Convex Accuracy*. Again, the higher the precision, the 'more convex' each cell in the latent space seems to be. For a qualitative evaluation, we show this phenomenon in Figure 2 and stress that linear interpolations conserve the image class.

What happens when the number of modes m is strictly bigger than the dimension d . When the number of modes m exceeds the latent space dimension d , the problem becomes more complex and the Gaussian multi-bubble conjecture is no longer valid. In this generalized context, GANs could give hints on the geometry of the optimal partition. We show in Figure 3 examples when training a GANs from \mathbb{R}^2 to \mathbb{R}^m with m equidistant target points in \mathbb{R}^m . This could give some insights on how to divide the Gaussian space into m equitable areas with least Gaussian-weighted perimeter.

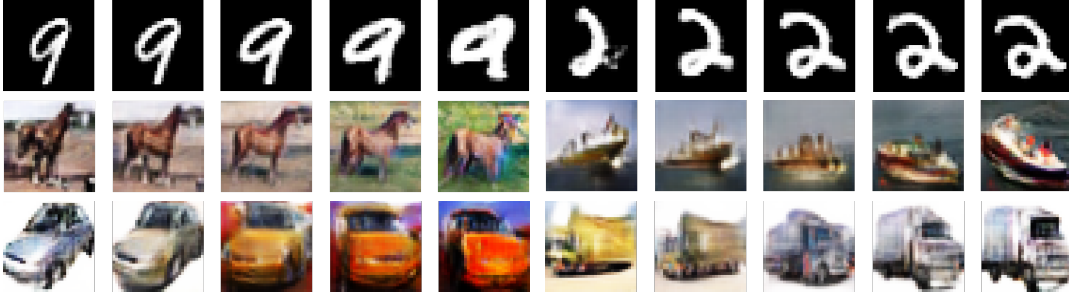


Figure 2: Illustration of convexity of classes in the latent space of GANs trained on MNIST and CIFAR-10. Visual inspection confirm that latent linear interpolations between two samples of the same class conserve the class.

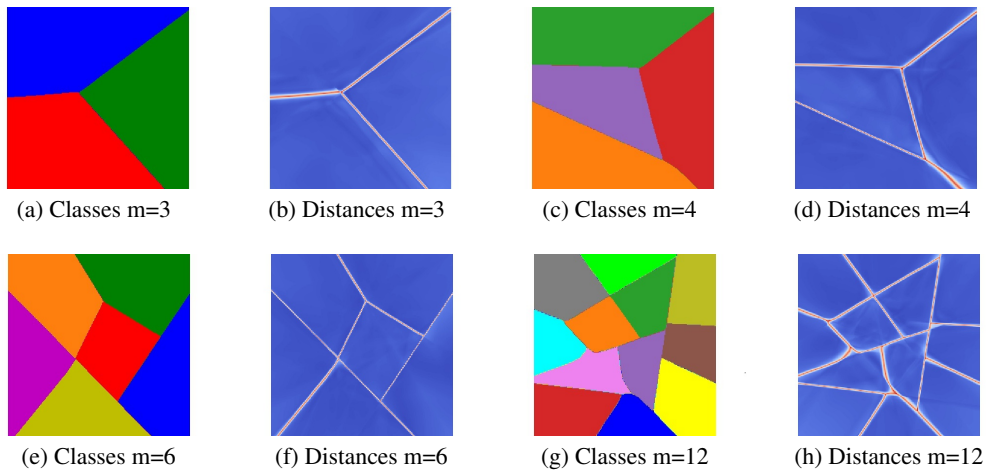


Figure 3: Extending the multi-bubble conjecture when $m > d + 1$. The *Classes* figures correspond to cells in the latent space: each cell maps to a distinct data point in the output space. The *Distances* figures correspond to heatmaps in the latent space of the distance to the nearest neighbor in the output space. We observe that each cell still verifies 1) flat sides 2) convexity.

4.2 Illustrating the impact of the latent dimension on the performance of GANs

To illustrate the phase transition showed in Corollary 2, we propose, for a fixed dataset, to vary the number of latent dimensions d from 2 to 128. In Figure 4, we exhibit two phases in the performance of GANs when changing the number of latent dimensions. When d is below a dataset-specific threshold, the precision of the model falls when reducing the number of latent dimensions. When d is above this threshold, the precision becomes constant, and increasing the number of latent dimensions does not bring any apparent improvement.

Interestingly, this experiment can reveal the complexity of the dataset and its intrinsic number of modes. We can observe that going from MNIST to CIFAR-10 and CIFAR-100, the phase transition appears for a larger number of dimension. Also, when comparing the different datasets, we observe that the more modes a dataset have, the lower the precision saturates. This is coherent with our Corollary 2, where the precision decreases w.r.t. to the number of modes in $\sqrt{\log(m)}$ when $m \leq d$.

Disentangling the manifold dimension from the number of modes. A caveat of the previous experiment is that it is difficult to interpret the loss in performance of the model. Indeed, one cannot easily know whether this loss is due to:

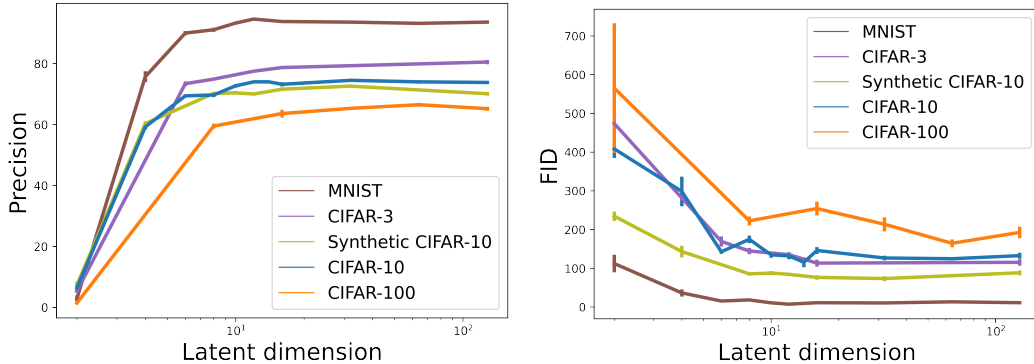


Figure 4: Performance of GANs w.r.t. the number of latent space dimensions. On the left, the precision consistently improves when the latent dimension increases. On the right, the FID gets lower with increased latent dimension. Obviously, a simpler dataset (MNIST) leads to a higher precision and a lower FID. Confidence intervals are computed on different checkpoints of a single run. FID computed with dataset-specific classifier (Naeem et al., 2020; Kynkäänniemi et al., 2022).

- *density misspecification* (Roth et al., 2017): in this case, fitting a disconnected manifold with a unimodal distribution.
- *dimensional misspecification* (Roth et al., 2017): having a latent dimension that does not match the intrinsic dimensionality of the target distribution.

To do so, we propose to control the intrinsic dimensionality of the data by generating a synthetic disconnected distributions using conditional GANs pre-trained on CIFAR-10.

We thus design an experiment that allows us to ensure that phase transition comes from the number of modes in the data and not from the intrinsic dimensionality of the data manifold. Let us consider a dataset with discrete class labels. We train a conditional GAN $G_{\theta}^c(z, y)$ with a very low-dimensional latent space \mathbb{R}^d , e.g. \mathbb{R}^3 in our experiments. This enforces the intrinsic dimension d_m of each mode of the distribution to $d_m \leq d$. Then, we train unconditional GANs G_{θ} on the distribution learned by the conditional GAN, vary the number of latent dimensions of G_{θ} , and plot the performance of these different models with respect to the synthetic distribution. We create synthetic datasets on *CIFAR-10* and name it *Synthetic CIFAR-10* in Figure 4.

To evaluate the performance of GANs, we use FID (Heusel et al., 2017), the improved precision metric (Kynkäänniemi et al., 2019). Other metrics improved recall, and the density/coverage (Naeem et al., 2020) are also given in Appendix. As recommended by recent works (Naeem et al., 2020; Kynkäänniemi et al., 2022), we use a dataset-specific classifier to extract image features instead of an ImageNet pre-trained classifier. We observe that both the precision and the FID of the trained generators increase with the latent dimension until reaching a plateau that is a function of the complexity of the dataset. This is consequently on par with the findings of Corollary 2.

5 Conclusion

In this paper, we aim at making a step towards a better understanding of GANs learning disconnected distributions. When the latent space dimension is large enough, we explicit the optimal latent space geometry of GANs: ‘simplicial clusters’, a Voronoi partition where each cell is a convex cone. We further show experimentally that GANs with sufficient latent capacity tend to respect this optimal geometry. We believe that our analysis can foster exciting research on GANs, with both theoretical and practical impacts. For example, understanding the geometry of the optimal latent space could help in designing semi-supervised or transfer algorithms from GANs. Also, it could inspire new neural architectures with a bias for this ‘simplicial cluster’ partitioning of the latent space.

Limitations. A first limitation of our work is that we do not have a convergence analysis: what are the conditions under which GANs converge to a simplicial cluster partition of the latent space? It could be interesting to connect this with overparametrization in GANs, which was shown to facilitate

GANs convergence (Balaji et al., 2020). A second limitation is that our lower-bound on optimal GANs is non-tight in the case $d < m$, because the minimizers of Gaussian isoperimetric inequalities are not known in this case.

Potential negative societal impacts. This work is mainly about understanding the behavior of deep generative models. Thus, it can lead to practical improvements in this technology and increase its potential negative impacts. Potential negative impacts of deep generative models are mainly linked to those of *deepfakes* (Fallis, 2020).

References

- Rameen Abdal, Peihao Zhu, Niloy J Mitra, and Peter Wonka. Labels4free: Unsupervised segmentation using stylegan. In *Proceedings of the IEEE/CVF International Conference on Computer Vision*, pages 13970–13979, 2021. (Cited on 1)
- M. Arjovsky, S. Chintala, and L. Bottou. Wasserstein generative adversarial networks. In D. Precup and Y.W. Teh, editors, *Proceedings of the 34th International Conference on Machine Learning*, volume 70, pages 214–223. PMLR, 2017. (Cited on 3, 7)
- Georgios Arvanitidis, Lars Kai Hansen, and Søren Hauberg. Latent space oddity: on the curvature of deep generative models. In *International Conference on Learning Representations*, 2018. (Cited on 3)
- Samaneh Azadi, Catherine Olsson, Trevor Darrell, Ian Goodfellow, and Augustus Odena. Discriminator rejection sampling. In *International Conference on Learning Representations*, 2018. (Cited on 3)
- Yogesh Balaji, Mohammadmahdi Sajedi, Neha Mukund Kalibhat, Mucong Ding, Dominik Stöger, Mahdi Soltanolkotabi, and Soheil Feizi. Understanding over-parameterization in generative adversarial networks. In *International Conference on Learning Representations*, 2020. (Cited on 10)
- Gérard Biau and Luc Devroye. *Lectures on the nearest neighbor method*. Springer, 2015. (Cited on 17)
- Ralph P Boland and Jorge Urrutia. Separating collections of points in euclidean spaces. *Information Processing Letters*, 53(4):177–183, 1995. (Cited on 6, 21)
- A. Brock, J. Donahue, and K. Simonyan. Large scale GAN training for high fidelity natural image synthesis. In *International Conference on Learning Representations*, 2019. (Cited on 3)
- Nutan Chen, Alexej Klushyn, Richard Kurle, Xueyan Jiang, Justin Bayer, and Patrick Smagt. Metrics for deep generative models. In *International Conference on Artificial Intelligence and Statistics*, pages 1540–1550. PMLR, 2018a. (Cited on 3)
- Ting Chen, Mario Lucic, Neil Houlsby, and Sylvain Gelly. On self modulation for generative adversarial networks. In *International Conference on Learning Representations*, 2018b. (Cited on 7, 15)
- Don Fallis. The epistemic threat of deepfakes. *Philosophy & Technology*, pages 1–21, 2020. (Cited on 10)
- Herbert Federer. *Geometric measure theory*. Springer, 1969. (Cited on 20)
- I. Goodfellow, J. Pouget-Abadie, M. Mirza, B. Xu, D. Warde-Farley, S. Ozair, A. Courville, and J. Bengio. Generative adversarial nets. In Z. Ghahramani, M. Welling, C. Cortes, N.D. Lawrence, and K.Q. Weinberger, editors, *Advances in Neural Information Processing Systems 27*, pages 2672–2680. Curran Associates, Inc., 2014. (Cited on 1, 3)

- I. Gulrajani, F. Ahmed, M. Arjovsky, V. Dumoulin, and A.C. Courville. Improved training of Wasserstein GANs. In I. Guyon, U. von Luxburg, S. Bengio, H. Wallach, R. Fergus, S. Vishwanathan, and R. Garnett, editors, *Advances in Neural Information Processing Systems 30*, pages 5767–5777. Curran Associates, Inc., 2017. (Cited on 3, 7)
- Swaminathan Gurumurthy, Ravi Kiran Sarvadevabhatla, and R Venkatesh Babu. Deligan: Generative adversarial networks for diverse and limited data. In *Proceedings of the IEEE conference on computer vision and pattern recognition*, pages 166–174, 2017. (Cited on 3)
- Erik Härkönen, Aaron Hertzmann, Jaakko Lehtinen, and Sylvain Paris. Ganspace: Discovering interpretable gan controls. *Advances in Neural Information Processing Systems*, 33:9841–9850, 2020. (Cited on 3)
- Kaiming He, Xiangyu Zhang, Shaoqing Ren, and Jian Sun. Deep residual learning for image recognition. In *Proceedings of the IEEE conference on computer vision and pattern recognition*, pages 770–778, 2016. (Cited on 7)
- Steven Heilman, Aukosh Jagannath, and Assaf Naor. Solution of the propeller conjecture in \mathbb{R}^3 . *Discrete & Computational Geometry*, 50(2):263–305, 2013. (Cited on 2)
- M. Heusel, H. Ramsauer, T. Unterthiner, B. Nessler, and S. Hochreiter. Gans trained by a two time-scale update rule converge to a local nash equilibrium. In *Advances in Neural Information Processing Systems*, pages 6626–6637, 2017. (Cited on 9, 15)
- Yifan Jiang, Shiyu Chang, and Zhangyang Wang. Transgan: Two pure transformers can make one strong gan, and that can scale up. *Advances in Neural Information Processing Systems*, 34, 2021. (Cited on 1)
- Olav Kallenberg. *Foundations of modern probability*. Springer Science & Business Media, 2006. (Cited on 17)
- T. Karras, S. Laine, and T. Aila. A style-based generator architecture for generative adversarial networks. In *Proceedings of the IEEE Conference on Computer Vision and Pattern Recognition*, pages 4401–4410, 2019. (Cited on 1, 3)
- Mahyar Khayatkhoei, Maneesh K Singh, and Ahmed Elgammal. Disconnected manifold learning for generative adversarial networks. In *Advances in Neural Information Processing Systems*, pages 7343–7353, 2018. (Cited on 1, 3)
- N. Kodali, J. Abernethy, J. Hays, and Z. Kira. On convergence and stability of GANs. *arXiv.1705.07215*, 2017. (Cited on 3)
- Alex Krizhevsky, Geoffrey Hinton, et al. Learning multiple layers of features from tiny images. 2009. (Cited on 7)
- T. Kynkäänniemi, T. Karras, S. Laine, J. Lehtinen, and T. Aila. Improved precision and recall metric for assessing generative models. In H. Wallach, H. Larochelle, A. Beygelzimer, F. d’Alché Buc, E. Fox, and R. Garnett, editors, *Advances in Neural Information Processing Systems 32*, pages 3927–3936. Curran Associates, Inc., 2019. (Cited on 1, 2, 3, 4, 9, 15)
- Tuomas Kynkäänniemi, Tero Karras, Miika Aittala, Timo Aila, and Jaakko Lehtinen. The role of imagenet classes in fr\`echet inception distance. *arXiv preprint arXiv:2203.06026*, 2022. (Cited on 9)
- Y. LeCun, L. Bottou, Y. Bengio, and P. Haffner. Gradient-based learning applied to document recognition. In *Proceedings of the IEEE*, pages 2278–2324, 1998. (Cited on 7)
- Michel Ledoux. Isoperimetry and gaussian analysis. In *Lectures on probability theory and statistics*, pages 165–294. Springer, 1996. (Cited on 2, 5)

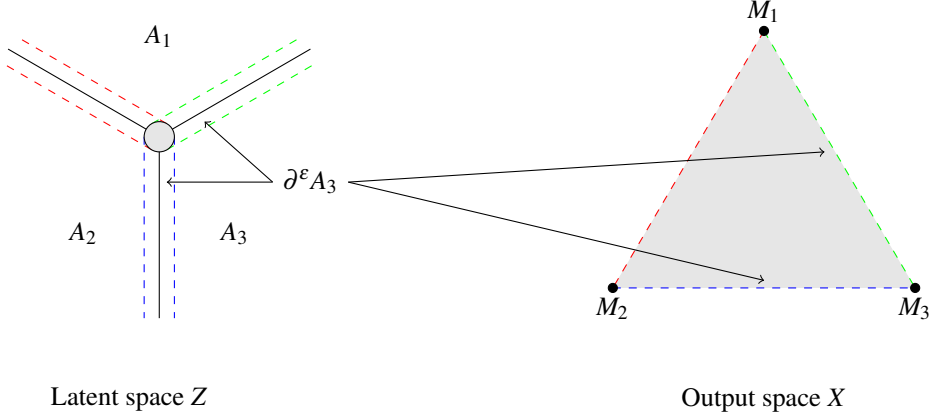
- Emanuel Milman and Joe Neeman. The gaussian double-bubble and multi-bubble conjectures. *Annals of Mathematics*, 195(1):89–206, 2022. (Cited on [5](#), [6](#), [7](#), [19](#), [20](#))
- T. Miyato, T. Kataoka, M. Koyama, and Y. Yoshida. Spectral normalization for generative adversarial networks. In *International Conference on Learning Representations*, 2018. (Cited on [3](#))
- Muhammad Ferjad Naeem, Seong Joon Oh, Youngjung Uh, Yunjey Choi, and Jaejun Yoo. Reliable fidelity and diversity metrics for generative models. pages 7176–7185, 2020. (Cited on [1](#), [2](#), [3](#), [4](#), [9](#), [15](#))
- K. Roth, A. Lucchi, S. Nowozin, and T. Hofmann. Stabilizing training of generative adversarial networks through regularization. In I. Guyon, U. von Luxburg, S. Bengio, H. Wallach, R. Fergus, S. Vishwanathan, and R. Garnett, editors, *Advances in Neural Information Processing Systems 30*, pages 2018–2028. Curran Associates, Inc., 2017. (Cited on [9](#))
- M.S.M. Sajjadi, O. Bachem, M. Lucic, O. Bousquet, and S. Gelly. Assessing generative models via precision and recall. In S. Bengio, H. Wallach, H. Larochelle, K. Grauman, N. Cesa-Bianchi, and R. Garnett, editors, *Advances in Neural Information Processing Systems 31*, pages 5228–5237. Curran Associates, Inc., 2018. (Cited on [1](#), [3](#), [4](#))
- Axel Sauer, Katja Schwarz, and Andreas Geiger. Stylegan-xl: Scaling stylegan to large diverse datasets. *arXiv preprint arXiv:2202.00273*, 2022. (Cited on [3](#))
- Gideon Schechtman. Approximate gaussian isoperimetry for k sets. In *Geometric Aspects of Functional Analysis*, pages 373–379. Springer, 2012. (Cited on [5](#), [18](#), [21](#))
- Yujun Shen, Jinjin Gu, Xiaoou Tang, and Bolei Zhou. Interpreting the latent space of gans for semantic face editing. In *Proceedings of the IEEE/CVF Conference on Computer Vision and Pattern Recognition*, pages 9243–9252, 2020. (Cited on [1](#), [3](#))
- Ugo Tanielian, Thibaut Issenhuth, Elvis Dohmatob, and Jeremie Mary. Learning disconnected manifolds: a no gan’s land. In *International Conference on Machine Learning*, pages 9418–9427. PMLR, 2020. (Cited on [1](#), [3](#), [4](#), [5](#), [17](#))
- Aladin Virmaux and Kevin Scaman. Lipschitz regularity of deep neural networks: analysis and efficient estimation. In *Advances in Neural Information Processing Systems*, pages 3835–3844, 2018. (Cited on [3](#))
- X. Wei, B. Gong, Z. Liu, W. Lu, and L. Wang. Improving the improved training of Wasserstein GANs: A consistency term and its dual effect. In *International Conference on Learning Representations*, 2018. (Cited on [3](#))
- Zongze Wu, Dani Lischinski, and Eli Shechtman. Stylespace analysis: Disentangled controls for stylegan image generation. In *Proceedings of the IEEE/CVF Conference on Computer Vision and Pattern Recognition*, pages 12863–12872, 2021. (Cited on [1](#))
- Han Zhang, Ian Goodfellow, Dimitris Metaxas, and Augustus Odena. Self-attention generative adversarial networks. In Kamalika Chaudhuri and Ruslan Salakhutdinov, editors, *Proceedings of the 36th International Conference on Machine Learning*, volume 97 of *Proceedings of Machine Learning Research*, pages 7354–7363, 2019. (Cited on [3](#))
- Z. Zhou, J. Liang, Y. Song, L. Yu, H. Wang, W. Zhang, Y. Yu, and Z. Zhang. Lipschitz generative adversarial nets. In K. Chaudhuri and R. Salakhutdinov, editors, *Proceedings of the 36th International Conference on Machine Learning*, volume 97, pages 7584–7593. PMLR, 2019. (Cited on [3](#))

Checklist

1. (a) Do the main claims made in the abstract and introduction accurately reflect the paper's contributions and scope? [Yes]
(b) Did you describe the limitations of your work? [Yes], see Conclusion.
(c) Did you discuss any potential negative social impacts of your work? [Yes], see Conclusion.
(d) Have you read the ethics review guidelines and ensured that your paper conforms to them? [Yes]
2. If you are including theoretical results...
 - (a) Did you state the full set of assumptions of all theoretical results? [Yes]
 - (b) Did you include complete proofs of all theoretical results? [Yes]
3. If you ran experiments...
 - (a) Did you include the code, data, and instructions needed to reproduce the main experimental results (either in the supplemental material or as a URL)? [Yes], see Supplementary Material.
 - (b) Did you specify all the training details (e.g., data splits, hyperparameters, how they were chosen)? [Yes], see Supplementary Material.
 - (c) Did you report error bars (e.g., with respect to the random seed after running experiments multiple times)? [Yes], from different checkpoints of a single run.
 - (d) Did you include the total amount of compute and the type of resources used (e.g., type of GPUs, internal cluster, or cloud provider)? [Yes], see Supplementary material.
4. If you are using existing assets (e.g., code, data, models) or curating/releasing new assets...
 - (a) If your work uses existing assets, did you cite the creators? [Yes]
 - (b) Did you mention the license of the assets? [Yes]
 - (c) Did you include any new assets either in the supplemental material or as a URL? [No], we only use very standard datasets.
 - (d) Did you discuss whether and how consent was obtained from people whose data you're using/curating? [No], we only use very standard datasets.
 - (e) Did you discuss whether the data you are using/curating contains personally identifiable information or offensive content? [No], we only use very standard datasets.
5. If you used crowdsourcing or conducted research with human subjects...
 - (a) Did you include the full text of instructions given to participants and screenshots, if applicable? [N/A]
 - (b) Did you describe any potential participant risks, with links to Institutional Review Board (IRB) approvals, if applicable? [N/A]
 - (c) Did you include the estimated hourly wage paid to participants and the total amount spent on participant compensation? [N/A]

A Illustration of the optimal generator

We show an illustration of the optimal generator. Here, the optimal generator maps a 2-dimensional latent space Z to a 2-dimensional output space X with three modes (M_1, M_2, M_3) . Moreover, it separates the latent space with an optimal 'simplicial cluster' geometry. All the ε -boundaries intersect each other in the gray circle, which is thus mapped in the interior of the triangle (M_1, M_2, M_3) .



B Implementation details

Table 2: GANs training details on MNIST

Operation	Kernel	Strides	Feature Maps	Activation
Generator $G(z)$				
$z \sim N(0, I)$			$dim(z)$	
Fully Connected			$7 \times 7 \times 128$	
Convolution	3×3	1×1	$7 \times 7 \times 64$	LReLU
Convolution	3×3	1×1	$7 \times 7 \times 64$	LReLU
Nearest Up Sample			$14 \times 14 \times 64$	
Convolution	3×3	1×1	$14 \times 14 \times 32$	LReLU
Convolution	3×3	1×1	$14 \times 14 \times 32$	LReLU
Nearest Up Sample			$14 \times 14 \times 32$	
Convolution	3×3	1×1	$28 \times 28 \times 16$	LReLU
Convolution	3×3	1×1	$28 \times 28 \times 1$	Tanh
D(x)				
Convolution	4×4	2×2	$14 \times 14 \times 512$	LReLU
Convolution	3×3	1×1	$14 \times 14 \times 512$	LReLU
Convolution	4×4	2×2	$7 \times 7 \times 512$	LReLU
Convolution	3×3	1×1	$7 \times 7 \times 512$	LReLU
Fully Connected			1	-
Batch size	256			
Leaky ReLU slope	0.2			
Gradient Penalty weight	10			
Learning Rate Discriminator	1×10^{-4}			
Learning Rate Generator	5×10^{-5}			
Discriminator steps	2			
Optimizer	Adam	$\beta_1 : 0.5$	$\beta_2 : 0.5$	

Table 3: GANs training details on CIFAR datasets. BN stands for batch-normalization.

Operation	Kernel	Strides	Feature Maps	Conditional BN (Chen et al., 2018b)	Activation
Generator G(z)					
$z \sim N(0, Id)$			128		
Fully Connected			$4 \times 4 \times 128$	-	
ResBlock	$[3 \times 3] \times 2$	1×1	$4 \times 4 \times 128$	Y	ReLU
Nearest Up Sample			$8 \times 8 \times 128$	-	
ResBlock	$[3 \times 3] \times 2$	1×1	$8 \times 8 \times 128$	Y	ReLU
Nearest Up Sample			$16 \times 16 \times 128$	-	
ResBlock	$[3 \times 3] \times 2$	1×1	$16 \times 16 \times 128$	Y	ReLU
Nearest Up Sample			$32 \times 32 \times 128$	-	
Convolution	3×3	1×1	$32 \times 32 \times 3$	-	Tanh
Discriminator D(x)					
ResBlock	$[3 \times 3] \times 2$	1×1	$32 \times 32 \times 256$	-	ReLU
AvgPool	2×2	1×1	$16 \times 16 \times 256$	-	
ResBlock	$[3 \times 3] \times 2$	1×1	$16 \times 16 \times 256$	-	ReLU
AvgPool	2×2	1×1	$8 \times 8 \times 256$	-	
ResBlock	$[3 \times 3] \times 2$	1×1	$8 \times 8 \times 256$	-	ReLU
ResBlock	$[3 \times 3] \times 2$	1×1	$8 \times 8 \times 256$	-	ReLU
Mean spatial pooling	-	-	256	-	
Fully Connected			1	-	-
Batch size	256				
Gradient Penalty weight	10				
Learning Rate Discriminator	1×10^{-4}				
Learning Rate Generator	5×10^{-5}				
Discriminator steps	2				
Optimizer	Adam	$\beta_1 = 0.$	$\beta_2 = 0.999$		

Training. We use the Wasserstein loss, with gradient-penalty on interpolations of fake and real data. At each iteration, the discriminator is trained 2 steps and the generator 1 step with Adam optimizer. The batch size is 256. The learning rate of the discriminator is two times larger (Heusel et al., 2017), *i.e.* 5×10^{-5} for the generator and 1×10^{-4} for the discriminator. GANs are trained for 80k steps on MNIST and for 100k steps on CIFAR datasets. Architectures of generator and discriminator are described in Table 2 and Table 3.

Evaluation. Features are extracted with a classifier with simple architecture (convolutions, relu activation, no batch normalization). The classifier is trained on each dataset with cross-entropy loss. Weights of the classifiers are given in the code. For evaluation metrics, we follow the setting proposed by the authors. For FID (Heusel et al., 2017), we use 50k real images and 50k fake images. For precision, recall, density and coverage (Kynkäänniemi et al., 2019; Naeem et al., 2020), we use 10k real images and 10k fake images with nearest-k=5. Full results of the study on latent space dimension are presented in Table 4.

We also share the code for a better reproducibility.

GPUs. For all datasets, the training of GANs was run on NVIDIA TESLA V100 GPUs (16 GB). The training of a GAN for 100k steps on CIFAR takes around 30 hours.

Dataset	L. Dim.	Acc.	FD	Prec.	Rec.	Dens.	Cov.
MNIST	2	44.3 ± 2.5	112.3 ± 22.6	2.9 ± 1.0	89.1 ± 2.0	0.9 ± 0.3	2.1 ± 0.5
	4	59.4 ± 0.7	36.4 ± 9.3	75.7 ± 1.8	91.5 ± 0.5	47.9 ± 2.2	66.0 ± 2.0
	6	83.9 ± 0.4	15.4 ± 3.0	90.0 ± 0.7	92.4 ± 0.7	76.3 ± 2.0	85.8 ± 0.4
	8	84.7 ± 0.4	18.2 ± 3.4	91.1 ± 0.7	92.3 ± 0.5	81.3 ± 2.2	87.1 ± 0.8
	10	86.7 ± 0.4	10.7 ± 2.6	93.3 ± 0.5	91.5 ± 0.5	89.0 ± 2.2	89.8 ± 0.7
	12	87.4 ± 0.4	7.2 ± 1.6	94.6 ± 0.5	91.5 ± 0.5	94.3 ± 2.0	91.8 ± 0.7
	16	86.9 ± 0.4	11.0 ± 1.0	93.8 ± 0.3	91.8 ± 0.6	92.2 ± 0.9	90.7 ± 0.5
	32	90.3 ± 0.4	10.4 ± 1.6	93.6 ± 0.3	91.6 ± 0.7	91.8 ± 1.7	90.3 ± 0.6
	64	90.4 ± 0.3	13.3 ± 2.6	93.2 ± 0.4	92.3 ± 0.5	90.1 ± 2.0	90.2 ± 0.8
128	87.0 ± 0.4	11.0 ± 2.3	93.6 ± 0.3	91.8 ± 0.4	91.6 ± 1.5	90.4 ± 0.7	
CIFAR-10	2	19.1 ± 1.1	408.3 ± 23.3	6.4 ± 0.9	79.5 ± 1.3	1.8 ± 0.3	3.9 ± 0.4
	4	27.4 ± 1.0	298.6 ± 38.1	59.2 ± 0.8	78.9 ± 0.8	42.9 ± 0.6	65.9 ± 0.7
	6	42.7 ± 0.6	142.6 ± 5.4	69.4 ± 0.6	76.6 ± 0.5	60.3 ± 1.1	76.3 ± 0.8
	8	44.6 ± 0.6	174.7 ± 9.6	69.7 ± 0.7	79.6 ± 0.5	61.0 ± 1.4	77.8 ± 1.0
	10	53.7 ± 0.4	134.7 ± 7.4	72.7 ± 0.6	76.6 ± 0.6	67.6 ± 1.3	80.4 ± 1.0
	12	58.2 ± 0.3	131.8 ± 8.5	74.0 ± 0.5	76.1 ± 0.6	71.3 ± 1.6	82.0 ± 1.1
	14	60.1 ± 0.4	115.5 ± 12.7	74.0 ± 0.5	77.7 ± 0.8	72.4 ± 1.4	82.8 ± 0.9
	16	60.7 ± 0.4	145.9 ± 8.9	73.2 ± 0.7	78.5 ± 0.7	66.9 ± 1.3	79.6 ± 0.7
	32	63.5 ± 0.2	126.5 ± 5.9	74.5 ± 0.5	79.1 ± 0.4	70.9 ± 1.5	82.0 ± 0.9
64	64.0 ± 0.3	124.6 ± 4.5	74.0 ± 0.6	79.2 ± 0.3	71.2 ± 1.8	82.7 ± 1.0	
128	63.6 ± 0.4	132.6 ± 7.8	73.8 ± 0.5	79.2 ± 0.6	69.7 ± 1.2	82.1 ± 0.6	
CIFAR-100	2	10.7 ± 1.4	2826.7 ± 837.3	1.4 ± 0.2	70.2 ± 1.1	0.3 ± 0.1	0.7 ± 0.1
	8	15.2 ± 0.2	1112.3 ± 56.9	59.5 ± 0.8	62.8 ± 0.6	49.8 ± 1.6	70.5 ± 1.1
	16	21.8 ± 0.3	1270.9 ± 89.7	63.6 ± 1.3	61.3 ± 0.8	57.2 ± 2.8	73.9 ± 1.2
	32	23.9 ± 0.4	1068.0 ± 91.5	65.3 ± 0.4	62.1 ± 0.6	60.6 ± 1.1	77.4 ± 0.6
	64	25.1 ± 0.4	822.2 ± 50.5	66.5 ± 0.6	61.5 ± 0.8	64.0 ± 1.4	78.5 ± 0.8
	128	23.5 ± 0.3	963.0 ± 74.2	65.2 ± 0.7	62.2 ± 1.0	61.7 ± 1.6	77.4 ± 0.8
	256	21.2 ± 0.3	1086.6 ± 78.0	66.0 ± 0.5	60.2 ± 0.8	63.9 ± 1.2	78.1 ± 0.7
	512	20.6 ± 0.4	1128.7 ± 95.3	66.8 ± 0.6	61.1 ± 0.6	63.0 ± 1.2	77.6 ± 0.8
CIFAR-3	2	44.8 ± 2.0	473.9 ± 55.0	5.3 ± 0.5	69.9 ± 2.1	1.5 ± 0.2	2.7 ± 0.4
	6	72.4 ± 0.4	169.2 ± 13.1	73.4 ± 0.8	69.7 ± 1.5	65.6 ± 1.5	72.7 ± 1.3
	8	78.4 ± 0.5	144.6 ± 8.2	74.9 ± 0.5	72.5 ± 1.4	71.0 ± 1.6	75.8 ± 1.7
	12	80.6 ± 0.4	135.2 ± 6.4	77.5 ± 0.5	71.2 ± 1.3	76.5 ± 1.1	78.3 ± 1.7
	16	80.9 ± 0.3	113.3 ± 9.0	78.7 ± 0.5	71.8 ± 1.5	80.7 ± 1.4	80.4 ± 1.4
	128	80.6 ± 0.1	115.3 ± 8.4	80.5 ± 0.7	70.4 ± 1.7	87.1 ± 2.1	82.7 ± 1.3
Synthetic CIFAR-10	2	22.8 ± 2.2	234.6 ± 12.1	7.3 ± 1.3	71.7 ± 1.1	2.2 ± 0.4	4.6 ± 0.8
	4	33.8 ± 0.8	143.2 ± 15.0	60.3 ± 0.8	72.5 ± 0.8	44.4 ± 1.3	68.9 ± 1.2
	8	47.0 ± 0.6	85.5 ± 4.7	70.2 ± 0.3	72.5 ± 0.9	64.6 ± 0.6	83.2 ± 0.6
	10	52.6 ± 0.3	87.6 ± 5.4	70.4 ± 0.6	73.1 ± 0.7	66.2 ± 1.8	84.3 ± 0.7
	12	55.3 ± 0.4	84.3 ± 4.9	70.0 ± 0.5	73.5 ± 0.6	64.8 ± 1.2	83.6 ± 0.6
	16	59.1 ± 0.4	76.4 ± 6.1	71.6 ± 0.6	72.9 ± 1.2	68.7 ± 1.8	85.1 ± 0.4
	32	52.8 ± 0.2	73.4 ± 6.3	72.6 ± 0.5	72.2 ± 0.7	69.5 ± 1.4	85.7 ± 0.5
	128	58.7 ± 0.3	88.3 ± 6.2	70.1 ± 0.6	73.3 ± 0.6	66.3 ± 1.4	84.2 ± 0.8

Table 4: Performance of GANs when varying latent space dimension. Confidence intervals are computed on 10 checkpoints of the same training. See main paper for curves of precision and FID with regard to the latent space dimension.

C Technical results

C.1 Proof of Theorem 1

Lemma 2 (From [Tanielian et al. \(2020\)](#), Lemma 3). *Let μ be a probability distribution associated with a uniformly continuous probability density function f_μ . Assume that there exists constants $a_1 > 0, a_2 > 0$ such that for all $x \in E$, we have $a_1 < f_\mu(x) \leq a_2$. Then,*

$$\begin{aligned} R_{min} &\xrightarrow[n \rightarrow \infty]{} 0 \text{ a.s.} & \text{and} & & R_{min}^d &\xrightarrow[n \rightarrow \infty]{} \infty \text{ a.s.} \\ R_{max} &\xrightarrow[n \rightarrow \infty]{} 0 \text{ a.s.} & \text{and} & & R_{max}^d &\xrightarrow[n \rightarrow \infty]{} \infty \text{ a.s.} \end{aligned}$$

Coverage Let's prove ii) from Theorem 1.

Let μ be a probability distribution associated with a uniformly continuous probability density function f_μ such that there exists constants $a_1 > 0, a_2 > 0$ such that for all $x \in E$, we have $a_1 < f_\mu(x) \leq a_2$. Let ν be a singular probability distribution. Also, let D_μ, D_ν be datasets sampled from ν^n, μ^n . If μ is an estimator for ν , we want to show that:

$$\forall x \in D_\mu, \mathbb{1}_{\{\exists y \in D_\nu, y \in B_k(x)\}} \xrightarrow[k \rightarrow \infty]{} \mathbb{1}_{\text{supp}(\nu)}(x) \quad \text{in proba.} \quad (8)$$

$$(9)$$

where $B_k(X)$ refers to the set of k -nearest neighbor of the point X with respect to the Euclidean distance.

To begin with, let's assume that $x \notin S_\nu$. [Biau and Devroye \(2015, Lemma 2.2\)](#) have shown that

$$\lim_{n \rightarrow \infty} \|x_{(\varphi(n))} - x\| = \inf\{\|x - y\| \mid y \in S_\nu\} \quad \text{a.s.}$$

As S_ν is a closed set - e.g. [Kallenberg \(2006\)](#) - we have

$$\lim_{n \rightarrow \infty} \|x - x_{(\varphi(n))}\| > 0 \quad \text{a.s.}$$

and

$$\text{for all } y \in D_\nu, \lim_{n \rightarrow \infty} \|y - y_{(\varphi(n))}\| = 0 \quad \text{a.s.}$$

Thus, $\lim_{n \rightarrow \infty} \alpha_{\varphi(n)}^n(x) = 0 \quad \text{a.s.}$

Now, let's assume that $x \in S_\nu$. We want $\exists y \in S_\nu$ such that $\|x - y\| \leq \|x - x_{(k)}\|$. Noting $y_{(1)}$ the nearest neighbor within D_ν from x w.r.t. the Euclidean distance, this is equivalent to $\|x - y_{(1)}\| \leq \|x - x_{(k)}\|$.

Using [Biau and Devroye \(2015, Theorem 4.2\)](#), we have that:

$$\frac{k}{nV_d \|x - x_{(k)}\|^d} \rightarrow f_\nu(x),$$

where f_ν denotes the density function and V_d the volume of the unit sphere in \mathbb{R}^d . Thus,

$$\|x - x_{(k)}\| = \mathcal{O}\left(\left(\frac{k}{n}\right)^{1/d}\right).$$

Using [Biau and Devroye \(2015, Theorem 2.2\)](#), we have that:

$$\|x - y_{(1)}\| = o(n^{1/d}).$$

Thus, we conclude.

Density The first claim i) of Theorem 1 is a direct consequence from [Biau and Devroye \(2015, Lemma 20.5\)](#).

C.2 Proof of Lemma 1

Proof by contradiction. Assume that there exists a generator $G \in \mathcal{G}_L^{\mathcal{A}}$ such that $\alpha_G > 1 - \delta^{\varepsilon_{\min}, \mathcal{A}}$. We have

$$\partial^{\varepsilon_{\min}} \mathcal{A} = \bigcup_{i=1}^m (\cup_{j \neq i} A_j)^{\varepsilon_{\min}} \setminus (\cup_{j \neq i} A_j),$$

Let $z \in (\cup_{j \neq i} A_j)^{\varepsilon_{\min}} \setminus (\cup_{j \neq i} A_j)$ such that $G(z) = M_i$. We know that G is associated with \mathcal{A} , thus there exists z' and $j \in [1, m]$ such that $\|z - z'\| < \varepsilon_{\min}/2$ and $\|G(z) - G(z')\| \geq \|M_j - M_i\|/2$. Thus,

$$\frac{\|G(z) - G(z')\|}{\|z - z'\|} > \|M_j - M_i\|/\varepsilon_{\min} \geq L.$$

This contradicts G being in $\mathcal{G}_L^{\mathcal{A}}$.

C.3 Proof of Corollary 1

Let L, d be such that $L \geq d\sqrt{\log(m)}$. Let's prove that for any well-balanced generator $G \in \mathcal{G}_L$ verifying $\beta_G = 1$, we have:

$$\alpha_G \leq 1 - \varepsilon_{\min}(1 - \varepsilon_{\min}\sqrt{2\log(m)})/(\sqrt{2\pi})$$

Using [Schechtman \(2012\)](#), we have that:

$$\begin{aligned} \gamma\left((\cup_{j \neq i} A_j)^{\varepsilon} \setminus (\cup_{j \neq i} A_j)\right) &\geq \frac{1}{\sqrt{2\pi}} \int_{\varepsilon}^{\varepsilon+t} e^{-s^2/2} ds, \quad \text{where } t \text{ is such that } \frac{1}{\sqrt{2\pi}} \int_t^{\infty} e^{-s^2/2} ds = 1/m, \\ &\geq \frac{\varepsilon}{\sqrt{2\pi}} e^{-(t+\varepsilon)^2}, \\ &\geq \frac{\varepsilon}{\sqrt{2\pi}} \frac{1}{k} e^{-\varepsilon^2/2 - \varepsilon t}, \\ &\geq \frac{\varepsilon}{k\sqrt{2\pi}} (1 - \varepsilon t) \quad (\text{by convexity}). \end{aligned}$$

Thus, we have that:

$$\begin{aligned} \gamma(\partial^{\varepsilon} \mathcal{A}) &= \sum_{i=1}^m \gamma\left((\cup_{j \neq i} A_j)^{\varepsilon} \setminus (\cup_{j \neq i} A_j)\right), \\ &\geq \frac{\varepsilon(1 - \varepsilon t)}{\sqrt{2\pi}}, \\ &\geq \frac{\varepsilon(1 - \varepsilon\sqrt{2\log(m)})}{\sqrt{2\pi}}. \end{aligned}$$

Thus, we have

$$\begin{aligned} \alpha_G &\leq 1 - \delta^{\varepsilon_{\min}, \mathcal{A}}, \\ &\leq 1 - \frac{\varepsilon_{\min}(1 - \varepsilon_{\min}\sqrt{2\log(m)})}{\sqrt{2\pi}}. \end{aligned}$$

C.4 Proof of Theorem 2

Proof that G_{ε}^* is well-balanced. We recall that a generator is *well-balanced* if it is associated with a partition $\mathcal{A} = \{A_1, \dots, A_m\}$ on \mathbb{R}^d verifying $\gamma(A_1) = \dots = \gamma(A_m) = 1/m$.

By construction (7), any $z \in A_i$, we have that $\arg \min_{j \in [1, m]} \|G(z) - M_j\| = i$, thus G_{ε}^* is associated with the optimal partition \mathcal{A}^* .

Besides, since the components of \mathcal{A}^* have equal-measure, *i.e.* $\gamma(A_1^*) = \dots = \gamma(A_m^*) = 1/m$, G_{ε}^* is well-balanced.

Proof that G_ε^* has recall of 1: $\beta_{G_\varepsilon^*} = 1$. Let's show that $\beta_{G_\varepsilon^*} = 1$. This means that for every $i \in [1, n]$, there exists z such that $G(z) = M_i$.

We know that G_ε^* is well-balanced and associated with \mathcal{A}^* . From (Milman and Neeman, 2022), we know that $A_i, i \in [1, m]$ is a convex cone. Since ε is fixed, there is necessarily $z \in A_i$ such that $z \notin (\cup_{j \neq i} A_j)^\varepsilon$. For this specific z , we have $G_\varepsilon^*(z) = M_i$.

Proof that G_ε^* is Lipschitz: $G_\varepsilon^* \in \mathcal{G}_L$. By definition from G^* , we have that its equilibrium is equal to 1 since $\gamma(A_1) = \dots = \gamma(A_m)$.

Then, let $i \in [1, n]$ since $L \geq d\sqrt{m}$, there exists $x_i \in A_i$ and $\eta \geq 0$ such that $\mathbb{B}(x_i, \eta) \subset (A_i \setminus \cup_{j \neq i} A_j)^\varepsilon$. Thus, for all $z \in \mathbb{B}(x_i, \eta)$, we have $G^*(z) = X_i$. Thus, coverage = 1.

Now, let's show that $G^* \in \mathcal{G}_L$. To begin with, we have $\mathbb{R}^d = \partial^\varepsilon \mathcal{A} \cup (\mathbb{R}^d \setminus \partial^\varepsilon \mathcal{A})$.

$$\mathbb{R}^d \setminus \partial^\varepsilon \mathcal{A} = \bigcup_{i=1}^n A_i \setminus ((\cup_{j \neq i} A_j)^\varepsilon \cap A_i),$$

and, we know that for each $i \in [1, n]$, $G^*(z)$ is constant and thus L -Lipschitz.

Now,

$$\partial^\varepsilon \mathcal{A} = \bigcup_{i=1}^n (\cup_{j \neq i} A_j)^\varepsilon \setminus (\cup_{j \neq i} A_j) = \bigcup_{\substack{S \in \mathcal{P}([1, n]) \\ \text{card}(S) \geq 2}} \bigcap_{i \in S} A_i^\varepsilon.$$

Now, let $S \in \mathcal{P}([1, n])$ with $\text{card}(S) = k \geq 2$. Let $z, z' \in S^2$. Let $\alpha = (\alpha_1, \dots, \alpha_k)$ and $\beta = (\beta_1, \dots, \beta_k)$ be two vectors, both in \mathbb{R}^k , such that for all $i \in [1, k]$:

$$\alpha_i = \frac{d(z, (A_i^\varepsilon)^\complement)}{\sum_{j \in \mathcal{A}_z} d(z, (A_j^\varepsilon)^\complement)} \quad \text{and} \quad \beta_i = \frac{d(z', (A_i^\varepsilon)^\complement)}{\sum_{j \in \mathcal{A}_{z'}} d(z', (A_j^\varepsilon)^\complement)}$$

We have that

$$\begin{aligned} \|G(z) - G(z')\| &= \|(1 - \sum_{i \neq 1} \alpha_i)X_1 - (1 - \sum_{i \neq 1} \beta_i)X_1 + \sum_{i \neq 1} \alpha_i X_i - \sum_{i \neq 1} \beta_i X_i\| \\ &= \|\sum_{i \neq 1} (\alpha_i - \beta_i)(X_1 - X_i)\| \\ &\leq \max_{(i, j) \in [1, n]^2} \|X_i - X_j\| \|\alpha - \beta\|, \\ &\leq \max_{(i, j) \in [1, n]^2} \|X_i - X_j\| \|h(z) - h(z')\|, \end{aligned}$$

where h is the function from $\mathbb{R}^d \rightarrow \mathbb{R}^k$ be defined as:

$$h(z) = \left(\frac{d(z, (A_1^\varepsilon)^\complement)}{\sum_{i \in \mathcal{A}_z} d(z, (A_i^\varepsilon)^\complement)}, \dots, \frac{d(z, (A_k^\varepsilon)^\complement)}{\sum_{i \in \mathcal{A}_z} d(z, (A_i^\varepsilon)^\complement)} \right).$$

We can write $h = f \circ g$ with f the function defined from $\mathbb{R}^d \rightarrow \mathbb{R}^k$ by

$$f(z) = \left(d(z, (A_1^\varepsilon)^\complement), \dots, d(z, (A_k^\varepsilon)^\complement) \right),$$

and g the function defined on $\mathbb{R}^k \setminus \{0\}$ by

$$g(z) = \frac{z}{\|z\|_1}$$

We have that f is a \sqrt{k} -Lipschitz functions (given that $z \mapsto d(z, (A_k^\varepsilon)^\complement)$ is 1-Lipschitz). Besides, we know that outside the ball $B_\varepsilon(0)$, the function g is $(1/\varepsilon)$ -Lipschitz.

Using the convexity function $z \mapsto \sum_{j \in \mathcal{A}_z} d(z, (A_j^\varepsilon))$ (as a sum of convex functions), we can show that for all $z \in \mathcal{A}_z$, we have that $f(z) \leq (k-1)\varepsilon$ and $f(z)$ is not $B_\varepsilon(0)$. Finally, the function h is $\frac{\sqrt{k}}{\varepsilon}$ -Lipschitz.

Thus, we have that:

$$\|G(z) - G(z')\| \leq \frac{d\sqrt{k}}{\varepsilon} \|z - z'\|,$$

with $d = \max_{(i,j) \in [1,n]^2} \|X_i - X_j\|$. Consequently, noting that $\varepsilon = \frac{d\sqrt{m}}{L}$, we have that:

$$\|G(z) - G(z')\| \leq L \|z - z'\|.$$

We consequently finally conclude on the Lipschitzness of G^* on \mathbb{R}^d .

Proving that $\alpha_{G_{\varepsilon_{\max}}^*} \geq 1 - \delta^{\varepsilon_{\max} \mathcal{A}^*}$. Let $z \in (\delta^{\varepsilon_{\max} \mathcal{A}^*})^c$. By construction of $G_{\varepsilon_{\max}}^*$, we have that $|S_z| = 1$ and consequently $G(z) \in \{M_1, \dots, M_n\}$. Consequently, it is clear that

$$\alpha_{G_{\varepsilon_{\max}}^*} \geq 1 - \delta^{\varepsilon_{\max} \mathcal{A}^*}.$$

Interestingly, this holds independently on the dimension d and the number of modes m .

Proving that: for $m \leq d+1$, for any $\delta > 0$, if L is large enough, then, for any well-balanced $G \in \mathcal{G}_L$ verifying $\beta_G = 1$ we have: $\alpha_G \leq \alpha_{G_{\varepsilon_{\max}}^*} + \delta$. We consider \mathcal{A} the partition associated with G . Let us first define the gaussian boundary measure P_γ of a partition \mathcal{A} of \mathbb{R}^d . For partitions with smooth boundaries, it coincides with the $(d-1)$ -dimensional gaussian measure of the boundary, defined as follows:

$$P_\gamma(\mathcal{A}) = \liminf_{\varepsilon \rightarrow 0} \frac{\gamma(\partial^\varepsilon \mathcal{A}) - \gamma(\mathcal{A})}{\sqrt{2/\pi\varepsilon}}$$

Moreover, for sets with smooth boundaries, we have from Federer (1969, Theorem 3.2.29):

$$\liminf_{\varepsilon \rightarrow 0} \frac{\gamma(\partial^\varepsilon \mathcal{A}) - \gamma(\mathcal{A})}{\sqrt{2/\pi\varepsilon}} = \lim_{\varepsilon \rightarrow 0} \frac{\gamma(\partial^\varepsilon \mathcal{A}) - \gamma(\mathcal{A})}{\sqrt{2/\pi\varepsilon}}$$

Let us denote \mathcal{A}^* a simplicial cluster partition, A a standard partition where $\gamma(A_i) = \gamma(A_i^*)$ for all i , and $\sum_i \gamma(A_i) = 1$. By the multi-bubble theorem (Milman and Neeman, 2022), simplicial clusters are the unique minimizers of the gaussian isoperimetric problem, thus:

$$\begin{aligned} P_\gamma(\mathcal{A}^*) &\leq P_\gamma(\mathcal{A}) \\ \lim_{\varepsilon \rightarrow 0} \frac{\gamma(\partial^\varepsilon \mathcal{A}^*)}{\varepsilon} &\leq \lim_{\varepsilon \rightarrow 0} \frac{\gamma(\partial^\varepsilon \mathcal{A})}{\varepsilon} \\ L_{\mathcal{A}} &\leq L_{\mathcal{A}^*} \end{aligned}$$

where $L_{\mathcal{A}} = \lim_{\varepsilon \rightarrow 0} \frac{\gamma(\partial^\varepsilon \mathcal{A}^*)}{\varepsilon}$ and $L_{\mathcal{A}^*} = \lim_{\varepsilon \rightarrow 0} \frac{\gamma(\partial^\varepsilon \mathcal{A}^*)}{\varepsilon}$.

Then, for any $\delta > 0$, there exists $\varepsilon' > 0$ such that, for any $\varepsilon < \varepsilon'$,

$$\left| \frac{\gamma(\partial^\varepsilon \mathcal{A}^*)}{\varepsilon} - L_{\mathcal{A}^*} \right| < \delta, \quad \left| \frac{\gamma(\partial^\varepsilon \mathcal{A})}{\varepsilon} - L_{\mathcal{A}} \right| < \delta \quad \text{and} \quad L_{\mathcal{A}^*} \leq L_{\mathcal{A}}$$

Thus, for any $\delta > 0$, there exists $\varepsilon' > 0$ such that, for any $\varepsilon < \varepsilon'$,

$$\gamma(\partial^\varepsilon \mathcal{A}^*) \leq \gamma(\partial^\varepsilon \mathcal{A}) + 2\delta\varepsilon \tag{10}$$

Besides, we know that

$$\alpha_G \leq 1 - \gamma(\partial^{\varepsilon_{\min}} \mathcal{A}) \quad \text{and} \quad \alpha_{G_{\varepsilon}^*} \geq 1 - \gamma(\partial^{\varepsilon_{\max}} \mathcal{A}^*)$$

Let ε_{\max} such that $\varepsilon_{\min} \leq \varepsilon_{\max} \leq \varepsilon'$. We have

$$\begin{aligned}
\alpha_G &\leq 1 - \gamma(\partial^{\varepsilon_{\min}} \mathcal{A}) \\
&\leq 1 - \gamma(\partial^{\varepsilon_{\min}} \mathcal{A}^*) + 2\delta\varepsilon_{\min} \quad \text{using (10)} \\
&\leq 1 - \gamma(\partial^{\varepsilon_{\min}} \mathcal{A}^*) + 2\delta\varepsilon_{\max} + \gamma(\partial^{\varepsilon_{\max}} \mathcal{A}^*) - \gamma(\partial^{\varepsilon_{\max}} \mathcal{A}^*) \\
&\leq \alpha_{G_\varepsilon^*} + 2\delta\varepsilon_{\max} + \gamma(\partial^{\varepsilon_{\max}} \mathcal{A}^*) - \gamma(\partial^{\varepsilon_{\min}} \mathcal{A}^*) \\
&\leq \alpha_{G_\varepsilon^*} + 2\delta\varepsilon_{\max} + \gamma(\partial^{\varepsilon_{\max}} \mathcal{A}^*) - 2L_{\mathcal{A}^*}\varepsilon_{\max} - \gamma(\partial^{\varepsilon_{\min}} \mathcal{A}^*) + 2L_{\mathcal{A}^*}\varepsilon_{\min} + 2L_{\mathcal{A}^*}(\varepsilon_{\max} - \varepsilon_{\min}) \\
&\leq \alpha_{G_\varepsilon^*} + 4\delta\varepsilon_{\max} + 2L_{\mathcal{A}^*}\varepsilon_{\max}, \\
&\leq \alpha_{G_\varepsilon^*} + \varepsilon_{\max}(4\delta + 2L_{\mathcal{A}^*}).
\end{aligned}$$

We conclude by choosing L big enough such that ε_{\max} is strictly smaller than $\frac{\delta}{4\delta + 2L_{\mathcal{A}^*}}$.

C.5 Proof of Corollary 2

The precision of G_ε^* is thus such that:

$$\alpha_{G_{\varepsilon_{\max}}^*} \geq 1 - \gamma(\partial^{\varepsilon_{\max}} \mathcal{A}).$$

However, since $\partial^\varepsilon \mathcal{A} \subset \bigcup_{i=1}^n A_i^\varepsilon$, we have that for any ε

$$\gamma(\partial^\varepsilon \mathcal{A}) \leq \sum_{i=1}^n \gamma(A_i^\varepsilon).$$

Using results from [Schechtman \(2012, Proposition 1\)](#), we have that

$$\gamma(A_i^\varepsilon) \leq \frac{\varepsilon}{2m} (\sqrt{\pi \log(m^2)} + O(\frac{\log(m)}{m}))$$

Thus, we have

$$\alpha_{G_{\varepsilon_{\max}}^*} \geq 1 - (\varepsilon_{\max}/\sqrt{2}) (\sqrt{\pi \log(m)} + O(\frac{\log(m)}{m})).$$

Now, let $n > d$. Consequently, for a fixed number of modes, we expect the precision to decrease when the dimension of the latent decreases. In particular, [Boland and Urrutia \(1995\)](#) have shown the number of hyperplanes h required to separate m points in a d Euclidean space is such that:

$$h \leq \lceil (m - 2^{\lceil \log(d) \rceil})/d \rceil + \lceil \log(d) \rceil$$

Consequently, the optimal boundary \mathcal{A}^* has a measure lower than the union one the extension of these h hyperplanes:

$$h\gamma(H^\varepsilon) \leq \frac{\log(d)\varepsilon}{\sqrt{2\pi}} + O(\frac{m\varepsilon}{d}).$$

Assuming that $\frac{m}{d} = o(\log(d))$, we have that the generator G_ε^* associated with \mathcal{A}^* is L -Lipschitz ([Theorem 2](#)) has the following lower-bound:

$$\begin{aligned}
\alpha_G &\geq 1 - \delta^\varepsilon(\mathcal{A}^*), \\
&\geq \frac{\varepsilon_{\max} \log(d)}{\sqrt{2\pi}} + O(\frac{m\varepsilon_{\max}}{d}).
\end{aligned}$$